TSR The Sedimentary Record
SEPM | Society for Sedimentary Geology

Alpheus, S., & Hajek, E. (2024). The Fate of Bars in Braided Rivers. *The Sedimentary Record*, *22*(1). https://doi.org/10.2110/001c.117787

Research Article

The Fate of Bars in Braided Rivers

Safiya Alpheus[1], Elizabeth Hajek[1]

[1] Department of Geosciences, Pennsylvania State University

Keywords: stratigraphic architecture, braided rivers, channel threads, braid bar, confluence, fluvial sedimentology, bar

https://doi.org/10.2110/001c.117787

The Sedimentary Record

Vol. 22, Issue 1, 2024

Ancient river deposits are important archives of past landscape conditions on planetary surfaces. On Earth, they host valuable groundwater, energy resources, and carbon-storage potential. Reconstructing details of paleochannel forms and movements refines our understanding of the controls on river behavior under different climate, landcover, and tectonic conditions, and improves predictions and models of subsurface reservoirs. While studies have shown detailed connections between channel kinematics and bar-deposit architecture in meandering river systems, similar connections between braided river movements and preserved braided river deposits have not been established. Here we explore the potential for connecting braided river deposits to paleochannel movements, form, and flow conditions, and we evaluate the controls on bar preservation using synthetic stratigraphy generated with a numerical morphodynamic model. We investigate how attributes of channel morphodynamics, like channel widening or braiding intensity, impact bar deposits' preservation, scale, geometry, and architecture. We then assess how the scale, preservation, and facies composition of bar deposits reflect formative flow conditions of the channel. Our results demonstrate that no diagnostic signature of braided channel morphodynamics is recorded in bar-deposit geometry, facies, or preservation patterns. Rather, the unique local history of thread movements combines stochastically to preserve or rework bar deposits, and the timing of channel avulsion is the dominant control on bar preservation. Our results also show that representative paleochannel flow conditions will likely be accurately reflected in aggregate observations of braid bar deposits within channel-belt sandbodies at a regional or member/formation scale. These results demonstrate the need for broad sampling and statistical approaches to subsurface prediction and paleo-flow reconstruction in ancient, braided river deposits.

INTRODUCTION

Ancient channel deposits are important archives of past landscape conditions on planetary surfaces. Reconstructing paleoflow conditions and paleochannel kinematics from river deposits provides opportunities to constrain ancient landscape conditions (e.g., Hartley & Owen, 2022; Holbrook & Wanas, 2014; Lyster et al., 2021, 2022; McLeod et al., 2023; Wood et al., 2023); understand river response to changes in climate, tectonics, and land cover (e.g., Barefoot et al., 2022; Foreman, 2014; Foreman et al., 2012; Ielpi et al., 2022; McMahon & Davies, 2018; Sharma et al., 2023); and predict the distribution and migration of subsurface fluids in alluvial basins (e.g., Bridge & Lunt, 2006; Guo et al., 2022; Lewis et al., 2018; B. Martin et al., 2021). Details about paleochannel movements are recorded in the geometry, arrangement and preservation character of bar deposits in ancient channel fills (e.g., Chamberlin & Hajek, 2019; Colombera et al., 2017; Durkin et al., 2017, 2018) and are useful in answering outstanding questions about channel mobility (e.g. Mohrig et al., 2000; Sahoo et al., 2020; Wickert et al., 2013), channel planform (e.g., Gibling, 2006; Hartley et al., 2015), and river response to flow variability (e.g., Sambrook Smith et al., 2010; Nicholas et al., 2016; Li et al., 2023). Additionally, the height of fully preserved clinoforms (Figure 1) is a proxy for paleo-flow depth (Hajek & Heller, 2012; Mohrig et al., 2000)—an essential parameter in reconstructing the paleohydraulic conditions of ancient rivers (e.g., Hartley et al., 2015; Hartley & Owen, 2022; Lyster et al., 2021, 2022; Mahon & McElroy, 2018). To this end, understanding the controls on channel-bar preservation is critical for accurately reconstructing and comparing the behavior and response of ancient rivers to different land cover, climate, and tectonic conditions.

Preservation of features like bedforms, barforms, and channels in fluvial deposits has been explored at a variety of scales in field, experimental, and numerical systems (e.g., Chamberlin & Hajek, 2019; Das et al., 2022; Fielding et al., 2018; Ganti et al., 2013; Leary & Ganti, 2020; Leclair et al., 1997; Reesink et al., 2015; van de Lageweg, Schuurman, et al., 2016). Previous theoretical, experimental and numerical studies have shown relationships between bedform height and the distribution of cross-set thicknesses (e.g., Bradley & Venditti, 2017; Bridge, 1997; Ganti et al.,

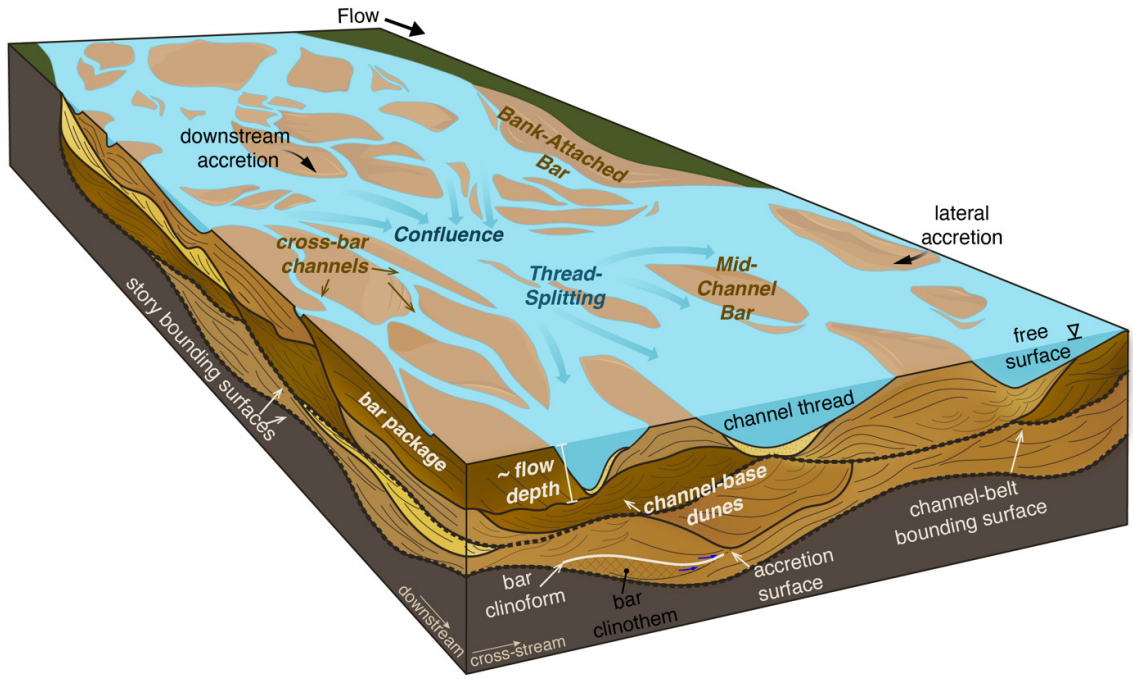

Figure 1. Conceptual diagram of a braided river and its stratigraphic deposits. Zones of thread confluence and thread splitting, shown by blue arrows, facilitate the formation, accretion, and deformation of bank-attached and mid-channel bars. Within a larger channel-belt sand body, bar deposits can be stratigraphically preserved as packages characterized by sigmoidal bar clinothems that accrete in the direction of bar growth and downlap (e.g., blue arrows in cross-stream stratigraphic view) onto older deposits.

2013; Jerolmack & Mohrig, 2005; Leclair et al., 1997; Paola & Borgman, 1991). At the bar scale, flow conditions and hierarchies of bed features (e.g., bedforms and bars) impact the relationship between preserved cross-strata and formative topography (e.g., Nicholas et al., 2016; Ganti et al., 2020; Sambrook Smith et al., 2019). At the largest scale in river networks, the frequency of channel avulsion and the nature of sediment supply to basins impacts channel-belt preservation and amalgamation (e.g., Cardenas et al., 2023; Chadwick et al., 2022; Chamberlin & Hajek, 2019; Heller & Paola, 1996; Strong et al., 2005).

Controls on the preservation of bar-scale deposits remain poorly understood for braided rivers. Bars are not explicitly captured at the experimental scales used to test theoretical and conceptual models about controls on bed-scale (e.g., Bradley & Venditti, 2021; Das et al., 2022; Ganti et al., 2013; Leary & Ganti, 2020) or landscape/channel-belt scale preservation (e.g., Chamberlin & Hajek, 2015, 2019; Heller & Paola, 1996; J. Martin et al., 2009; Paola et al., 2009; Straub & Wang, 2013). Consequently, bar preservation is studied using field observations and remote imagery of modern systems (e.g., Cardenas et al., 2020; Chamberlin & Hajek, 2019; Dixon et al., 2018; Rahman, 2023) and numerical models (e.g., Kleinhans & van den Berg, 2011; Schuurman & Kleinhans, 2015; Nicholas et al., 2016; Li et al., 2023; Sambrook Smith et al., 2019; van de Lageweg, Schuurman, et al., 2016; van de Lageweg, van Dijk, et al., 2016). These investigations have shown that channel-thread kinematics such as lateral migration, widening, thread-splitting, and confluence, influence the formation and morphology of bars in braided rivers (Figure 1). Furthermore, perturbations in flow and sediment supply across multiple scales (e.g., local-, reach-, and system-scale) can influence thread position and mobility, affecting the configuration and kinematics of channel threads and bars in braided rivers. This has been observed in systems where migrating and deforming bars and migrating threads alter local flow paths and network configurations (e.g., Dixon et al., 2018; Le Guern et al., 2023; Schuurman et al., 2016; Wintenberger et al., 2015), or where the configuration and migration behavior of bars and threads in braided networks is altered in response to flooding events and land-use change (e.g., Ghosh et al., 2023; Jarriel et al., 2021; Tejedor et al., 2022).

Despite careful work connecting braided river morphodynamics to bar morphology and migration (e.g., Ashworth et al., 2011; Fielding, 2022; Germanoski & Schumm, 1993; Lunt et al., 2004; Schuurman & Kleinhans, 2015) and detailed descriptions of ancient deposits (e.g., Barefoot et al., 2022; Bridge, 1993; Bridge & Lunt, 2006; Cardenas et al., 2020; Chamberlin & Hajek, 2019; Fielding et al., 2018; Lunt et al., 2004; Miall, 1988), specific connections between braided river kinematics and bar deposit preservation are lacking. Facies models suggest that braided river deposits are dominated by laterally extensive and amalgamated sand bodies that comprise multiple bar deposits, channel floor cross-strata and occasional pockets of low-flow or abandonment fines (Ashworth et al., 2011; Gibling, 2006; Hajek et al., 2010; Lynds & Hajek, 2006; Miall, 1985, 1988). The high degree of channel mobility in braided rivers suggests

that their deposits should be reworked, with common, truncated bar packages and amalgamated channel bodies (e.g., Ashworth et al., 2011; Best et al., 2003; Bridge & Lunt, 2006; Gibling, 2006; Wickert et al., 2013). In meandering systems, the geometry, preservation, and facies of point bar deposits can reflect specific channel kinematics like changing bend curvature, translation, or rotation, and chute or neck cutoffs, (e.g., Durkin et al., 2017, 2018; Smith et al., 2011; Sylvester et al., 2021). In braided rivers, thread migration and bifurcation have been observed to result in bar accretion, translation, deformation, and migration (e.g., Rice et al., 2009; Schuurman et al., 2013; Sambrook Smith et al., 2019). However, it is unclear whether braid bar preservation reflects specific channel movements, as shown for meandering systems. Additionally, the role of these movements in controlling channel-belt facies distribution in braided river deposits has not been fully explored. Deepening our understanding of the controls on braid bar preservation and stratigraphic architecture will improve our ability to generate nuanced facies models, compare modern, ancient, and model systems, and assess uncertainties associated with paleo-morphodynamic reconstructions (e.g., Holbrook & Wanas, 2014; Lyster et al., 2022; Mahon & McElroy, 2018)

Taken together, thread movements, channel kinematics, discharge variability, and intrinsic flow complexity in braided rivers impart stochasticity on bar formation, migration, and reworking. Here we explore the degree to which this stochasticity controls the fate of bars in braided rivers and our ability to reconstruct paleochannel conditions from ancient, braided river deposits. We used a physics-based morphodynamic model to investigate the baseline, autogenic statistics of bar preservation in a braided river under constant flow and sediment supply conditions. Using synthetic stratigraphy generated from the model, we evaluated how channel form and kinematics, including the degree of braiding and channel-belt widening, impact bar preservation. Using observations from synthetic stratigraphy that reflect field measurements obtainable from ancient outcrops, we identify field-scale observations and sampling strategies that can be particularly insightful for interpreting and reconstructing paleohydraulic conditions from ancient, braided river archives.

METHODS

We simulated the formation and evolution of a braided river under constant flow conditions using the numerical model, NAYS2DH, which solves two-dimensional, depth-averaged momentum and continuity equations over an orthogonal, curvilinear grid to simulate channelized flow and river-bed deformation (Asahi et al., 2013; Jang & Shimizu, 2005; Nelson et al., 2016; Shimizu et al., 2011). While we were not simulating conditions of any specific rivers, the model parameters we used broadly capture the dynamics of mid-sized, sand-bedded braided rivers and generate stratigraphic cross-sections with geometries and architectures reflective of many well-studied braided river deposits (e.g., Castlegate Sandstone, Kayenta Formation, Salt Wash Member of the Morrison Formation (e.g., Adams & Bhattacharya, 2005; McLaurin & Steel, 2007; Miall, 1988, 1994; Owen et al., 2015).The model was run over a 10 km long by 100 m wide initial grid with a slope of 0.001, and water discharge 100 m^3/s with random noise of up ± 0.5 m^3/s to maintain bar growth and decay. NAYS2DH is a transport-limited model in which sediment supply is determined by discharge (Shimizu et al., 2011); our model had a uniform sediment grain size of 0.31 mm. The model ran for 31.8 days with a morphodynamic scaling factor of 25, meaning the model simulated approximately 2.2 years (26 months) of activity output in 382 timesteps. It took the model 80 timesteps to reach a dynamic bed equilibrium (model spin-up time), and we ran the model for ~5x this initial bed equilibrium time. Our model run spanned approximately 32 times the average bar turnover timescale (Myrow et al., 2018)—estimated as the amount of time required to displace a bar in the downstream direction based on the unit sediment flux (Figure S2)—sufficient to completely rework the entire model bed multiple times throughout the run. The studied reach (1000 m to 9000 m) in the model domain was approximately 150 times as long as the average bar length. Processes like thread splitting and confluence, bar deposition, and channel widening arise spontaneously in the model, and thread and bar positions evolve and shift in ways that mimic multi-thread systems like in the Brahmaputra-Jamuna (e.g., Dixon et al., 2018; Rahman, 2023), Loire (e.g., Le Guern et al., 2023; Wintenberger et al., 2015), Sunwapta and South Saskatchewan rivers (e.g., Van Den Berg & Van Gelder, 1993) (Figure 2 Panel A). To end the run, we abruptly stopped the model simulating channel avulsion.

We built synthetic stratigraphic sections from the model by stacking channel-floor topography through time (Figure 2 Panel B). For each timestep at each bed location, we used local flow depth and velocity conditions to predict the stability of different bedforms (here referred to as '*pseudo-structures*') based on a representative experimental bedform-stability relationship (i.e. an example association between flow properties like shear stress, bed-material transport, and bed form) and the 0.31 mm grain size supplied in the model (Figure S1). We used these pseudo-structures to map bar facies onto these surfaces in the stratigraphic cross-sections (Figure 2 Panels B and C). Following the field-based mapping approach of Chamberlin and Hajek (2019), we defined lower bar facies as having higher-flow pseudo-structures like ripples, dunes and upper-stage plane bedding, and upper bar facies with lower-flow pseudo-structures such as lower-stage plane bedding and no movement. Bar-deposit packages were defined as conformable units of deposition bound by surfaces of non-deposition or erosion identified by downlap, onlap, offlap, and truncation stratal relationships (Figure 2 Panel C). We mapped bar packages in 33 cross-sections at a 250m spacing along the length of the model reach, excluding the first and last 1km stretches to avoid model-boundary effects.

For each bar package we characterized the degree of preservation using approaches previously used to classify bar preservation in ancient outcrops (Barefoot et al., 2022; Chamberlin & Hajek, 2019) where bar packages that con-

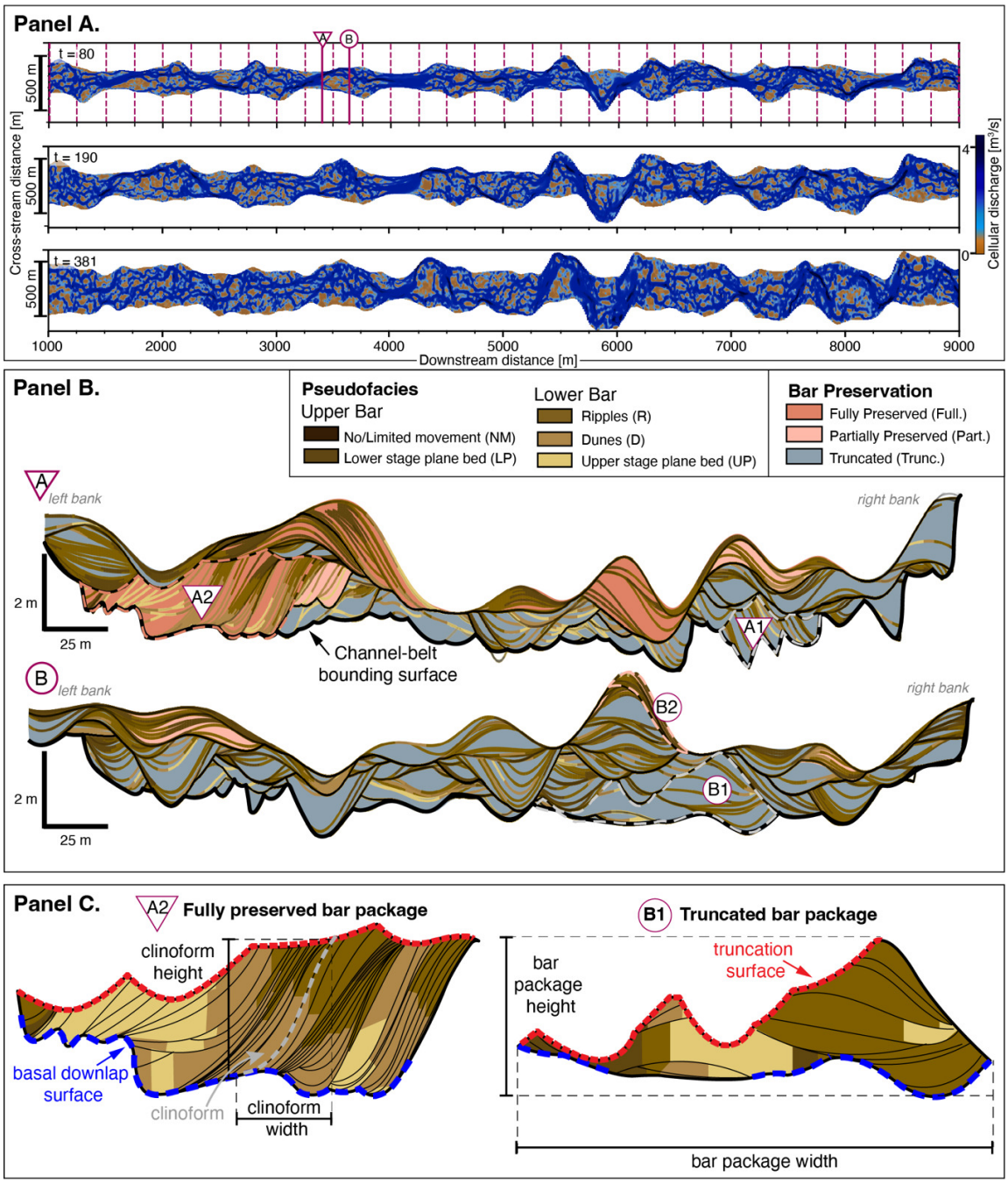

Figure 2. Braided river evolution and bar stratigraphic mapping from NAYS2DH morphodynamic model. Panel A: Model bed evolution at three timesteps: t = 80 (end-of model spin-up), t = 190 (model midpoint) and t = 381 (abandonment/model termination). Pink dashed lines in the top snapshot (t = 80) indicate locations of cross-sections mapped in this study, and solid lines indicate locations of two example cross sections: A (triangle) and B (circle) shown in panels below. The video of the complete model run is linked in the supplementary material. Panel B: Example model cross-sections A (triangle) and B (circle), fully mapped to illustrate bar packages, categorized by degree of bar preservation. Black lines outline bar-package bounding surfaces with internal bar surfaces (timelines) tracing bar evolution colored by modeled bar pseudo-structures assigned using relationships between bedform-stability and local flow conditions. Bar packages highlighted in Panel C and in Figure 5 are outlined with dashed lines (A1, A2, B1). Panel C: Example fully preserved (A2) and truncated (B1) bar packages filled in to show the distribution of modeled pseudo-structures within the clinothem packages. Both packages are outlined by their defining truncation (red) and basal downlap (blue) surfaces, and internal bar surfaces (clinoforms; black lines). Bar-package measurements (reported in Figure 4 and Figure S5) are defined including package height and width, and clinoform height and width.

tain both upper bar facies and bar-top rollover geometry are 'Fully Preserved' (Full.), packages with bar top rollover or upper bar facies are 'Partially Preserved' (Part.), and ones with neither upper-bar facies nor rollover are 'Truncated' (Trunc.) (Figure 2 Panels B and C). We measured the geometry (width, thickness, and area) and age of bar packages, and evaluated the deposition rate, and duration of deposition associated with each bar package. For each cross-section we compared bar-package preservation to aspects of braided network form and evolution including thread count, Entropic Braiding Index (eBI, Tejedor et al., 2022), and widening rate, to explore how these kinematics influence bar preservation.

RESULTS

Bar-package preservation is highly variable throughout the model deposits. Globally, truncated bars are the most abundant, accounting for 58% of the bar packages mapped in the model stratigraphy. However, the proportion of cross-sectional area composed of truncated versus partially and fully preserved bars varies among cross-section locations, reaching as high as 68% preserved (partially and fully preserved packages combined) and as low as 18% preserved (i.e. 82% truncated) in some cross-sections. We find no spatial trends along the river corridor~~.~~

Channel widening rate and braiding intensity (eBI) along the model reach (Figure 3A-C) show no relationship with bar preservation (Figure S3 & S4). For example, cross sections at 4000 m and 4250 m have similarly low widening rates (e.g., median = 0.18 m/timestep and 0.11 m/timestep respectively; Figure 3A) and comparable braiding intensities(e.g., median = 1.9 and 1.6 respectively; Figure 3B) but differ in total bar preservation by ~30% (Figure 3C). In contrast the median eBI value of the cross section at 5500 m is more than double that of the section at 5750 m (2.9 vs 1.1), for comparable widening rates (0.1 vs 0.6 m/timestep respectively; Figure 3A), but these sections have the similar preservation statistics between them (50% vs 59% preserved bars by area; Figure 3C).

The aggregate distribution of pseudo-structures on the bed and within the stratigraphic cross-sections bears no correlation to Entropic Braiding Index, widening rate, or the distribution and prevalence of preserved bars in cross-sections; some cross-sections dominated by truncated bar packages exhibit relatively high fractions of low-shear-stress conditions and others reflect mostly high-shear-stress conditions (Figure 3). Similarly, although partially and fully preserved bar packages, by definition, contain upper-bar facies that represent low-shear-stress conditions, there is no evidence of cross-sections with higher bar preservation showing a higher proportion of deposits reflecting low-shear-stress flow conditions (Figure 3). Overall, the stratigraphic cross-sections—relative to the time-integrated bed average flow conditions observed on the bed throughout the model run—are skewed toward high-shear-stress deposits (by cross-sectional area; Figure 3D, 3E). Bed conditions reflecting little sediment movement (No Movement and Lower-Stage-Plane-Bedding, Figure 3) are underrepresented in stratigraphic cross-sections by approximately 40% relative to their occurrence throughout the model run, and high-shear-stress conditions are overrepresented in cross-sections relative to their presence on the bed (dunes by 35% and upper-stage-plane bed by a factor of 2 relative to their occurrence on the model bed; Table S3.1).

Fully and partially preserved packages have larger areas, widths, and heights than most truncated packages (measurements exemplified in Figure 2C; Figure 4A-C); this pattern is also reflected in individual clinothem geometries (Figure 2C, Figure S5). Additionally, fully preserved packages are the youngest packages in the mapped model stratigraphy (Figure 4D, 4E). Fully preserved bar packages that are older than 100 model timesteps represent bar packages that have persisted in the channel for longer than the average bar turnover time (Figure S2). Partially preserved and truncated bar packages have a larger spread of ages in the record (Figure 4E), and the average sedimentation rates in fully preserved packages are higher than in partially preserved and truncated packages (Figure 4F).

Fully preserved bar packages scale with formative channel-thread geometry at their time of deposition (Figure 4G). Both the height of preserved clinothem and bar packages scale with the local maximum flow depth for fully and partially preserved deposits. Across all preservation categories, the maximum height of bar packages is generally greater than the height of the largest clinoform within the package, and package height scales with a greater proportion of the formative maximum flow depth associated with bar deposition than the clinoform height. On average, the heights of partially preserved and fully preserved bar packages represent 75% and 90% of the formative flow depth, where the average truncated package represents only 57% of the local maximum flow depth during the time of bar formation. We see no evidence of preservation bias based on initial bar size, with bar packages across all preservation categories spanning the range of formative flow depths in the model (Figure S5-G).

DISCUSSION

Our model simulates kinematics and morphodynamics similar to those observed in active braided rivers (e.g., Dixon et al., 2018; Rice et al., 2009; Tejedor et al., 2022) with simple boundary conditions (e.g. uniform grain size, constant discharge, and no vegetation interactions, and the synthetic stratigraphic architecture produced by the model reflects stratigraphic observations from braided ancient outcrops (e.g., Chamberlin & Hajek, 2019; Gibling, 2006; Miall, 1988). While finer computation scales, a spectrum of grain sizes, and channel-floodplain coupling could provide higher resolution detail about braided river kinematics and morphodynamics, our simplified model experiment provides robust insight into the baseline behavior of unperturbed braided systems, and allows for general insight into how bar deposits are preserved, and the degree to which they reflect river flow conditions.

Our results show that there is a spectrum of bar preservation in braided river deposits that varies spatially and is uncorrelated with time-averaged flow conditions in the channel. The shape, proportion, facies, and spatial distrib-

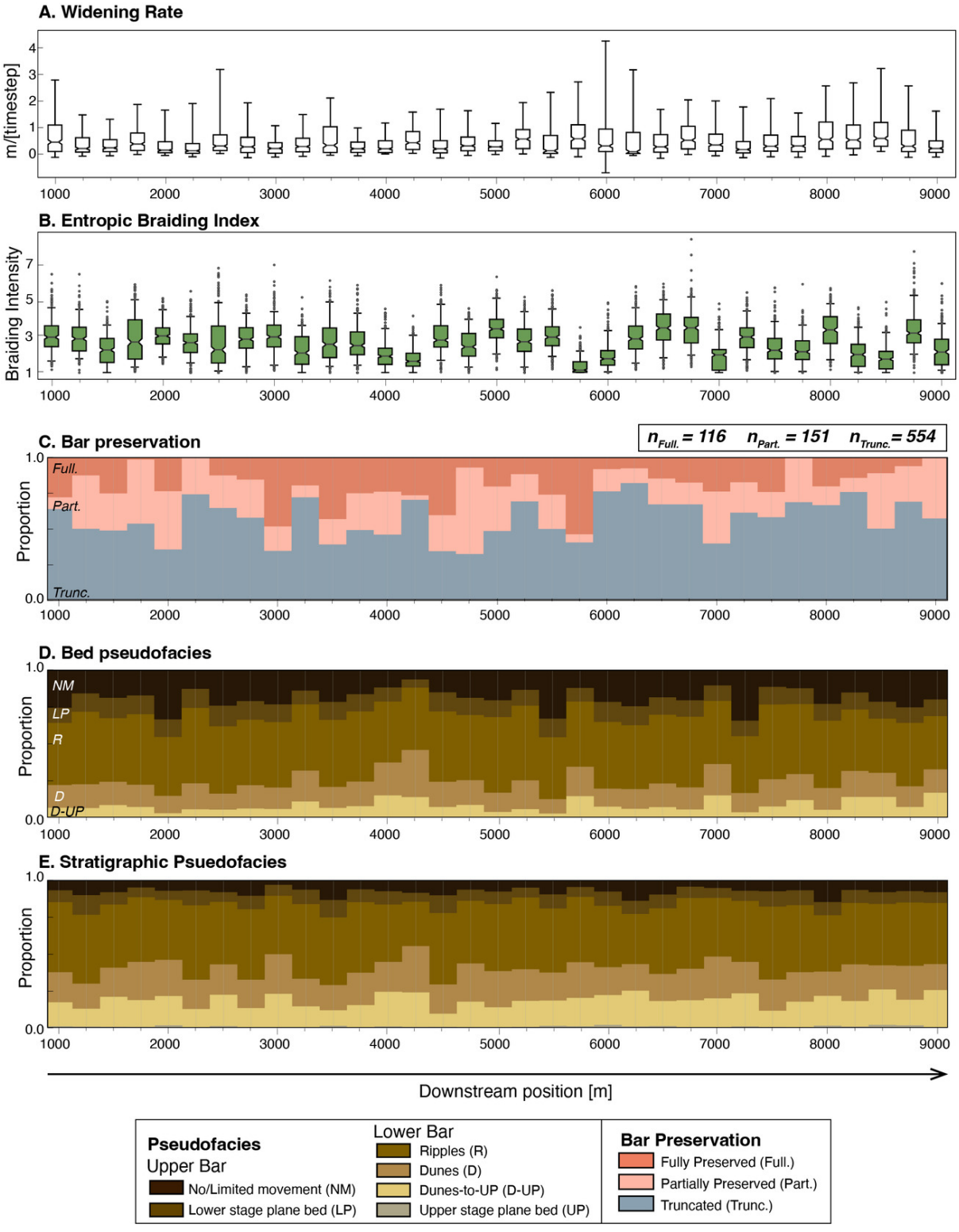

Figure 3. Distribution of (A) channel-belt widening, and (B) Entropic Braiding Index at each mapped cross-section location (250 m apart) from t= 80to end of model run. (C) Proportion of mapped stratigraphic cross-section area occupied by fully preserved (Full.), partially preserved (Part.) and truncated (Trunc.) bar deposits. (D) Time-integrated bed area at each cross-section location occupied by different pseudo-structures (averaged from t= 80to the end of the model run); NM – No movement, LP – Lower stage plane bedding, R – Ripples, D – Dunes, D-UP – Dunes to Upper Stage Plane Bedding, and UP – Upper stage plane bedding). (E) Proportion of different pseudo-structures by area in each stratigraphic cross section.

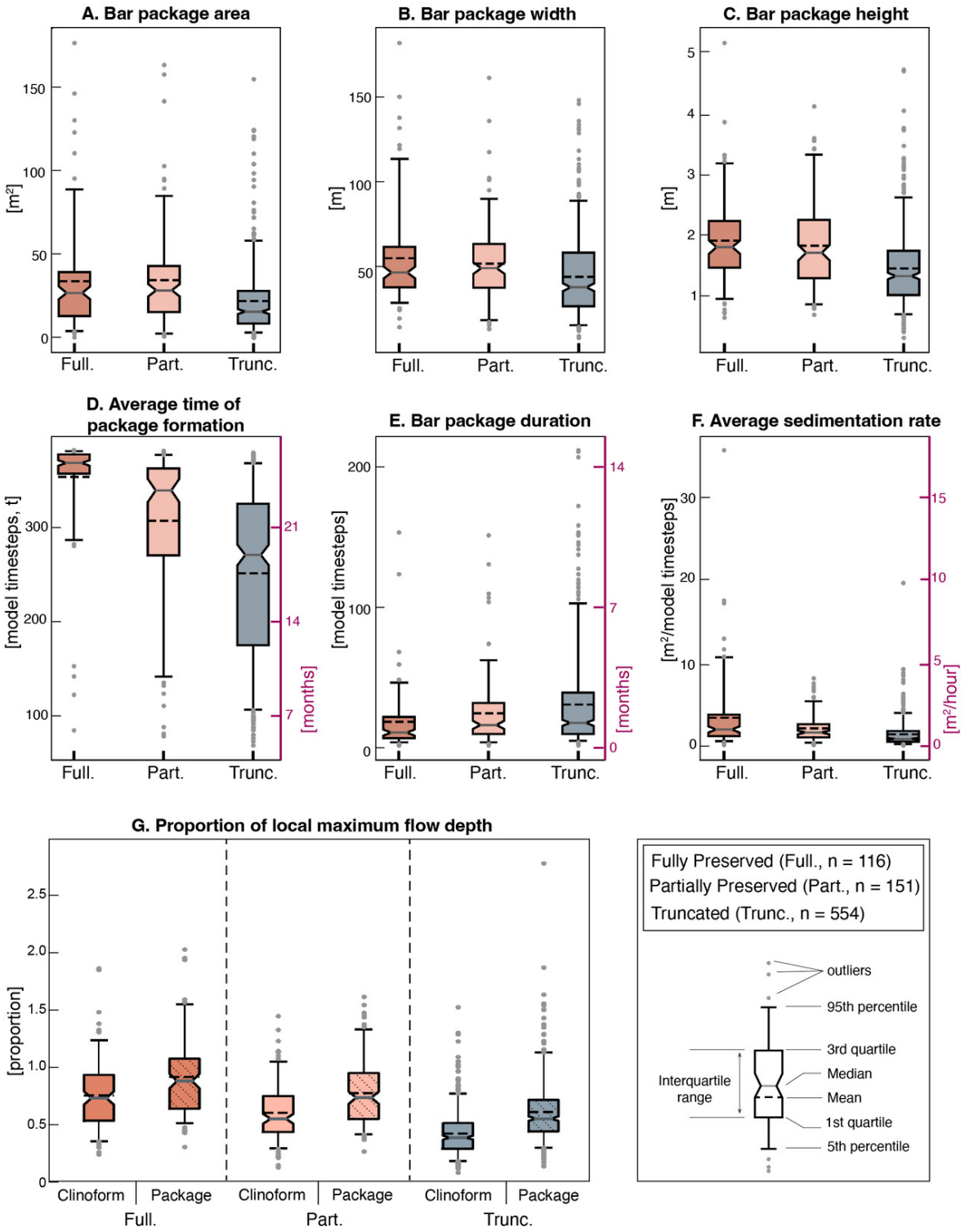

Figure 4. Geometric (A-C), age (D-F) and hydraulic characteristics (G) of fully, partially preserved, and truncated bar packages mapped in the model domain. Secondary axes (pink) in plots D-F show model timesteps converted to morphodynamic timescales (months and hours). (G) shows the distribution of clinoform and bar-package maximum relief divided by local maximum flow depth associated with the formation of the bar package for each preservation category. Inset key (lower right) describes how box and whisker plots are defined.

ution of bar preservation show no relationship to channel morphodynamics such as widening and braiding intensity. Fully and partially preserved packages generally occupy the same range of sizes and shapes as each other, and their thickness closely approximates the local maximum flow depth under which they formed. Truncated packages are generally smaller and only represent roughly half (57%) of their maximum formative flow depth. Additionally, our re-

sults highlight that the key difference between packages across preservation gradients is age, where fully preserved packages tend to be young. These results indicate that, while it may be difficult to reconstruct specific kinematics from ancient, braided river deposits, measurements of bars from braided paleochannels can be useful for 1) assessing the role of channel-belt avulsion (abandonment) on ancient landscapes, 2) comparing paleo-flow conditions across different systems, and 3) contextualizing and comparing braided river facies interpretations and paleohydraulic reconstructions from ancient deposits.

Controls on bar preservation in braided river deposits

In the model domain, morphodynamics, like channel-belt widening and thread migration, facilitate deposition and growth of bar packages however, preservation of these features is entirely dependent on what happens after a bar package is deposited (Figure 5). Each point on the bed experiences a unique, stochastic succession of channel kinematics that controls whether bar packages are preserved or truncated in the model stratigraphy. For example, in section A (Figure 5), packages A1 and A2 both formed during channel belt-widening events, during which bars accreted to fill lateral accommodation space created by retreating banks, but have different post-depositional histories. Package A1 was followed by a period of reworking via mobile threads, which generated a series of local deposition and erosion events. In contrast, deposition of package A2 was followed by a hiatus resulting from long-term thread abandonment (Figure 5). In contrast, section B, approximately one channel-width downstream, experienced an independent deposition-erosion history which produced a completely different stratigraphic architecture that lacks well-preserved bars (Figure 5). At this location, localized erosion and deposition events occurred across most of the channel width throughout most of the model duration; even when bars were deposited (e.g., B1), and channel activity was pervasive and dynamic enough to erode all but the youngest bar packages. Note that bar B1 was truncated by a sustained, localized erosion event, whereas bar A1 was truncated through a protracted period of alternating episodes of erosion and deposition. Furthermore, there is no trend between bar deposition or erosion and local channel braiding index or widening rate (Figure 5; Figure S3 and S4). Each cross section experiences the full, representative range of entropic braiding index (eBI) values and widening rates observed throughout the model run, but there is no consistency between phases of bar formation and preservation and eBI or widening rate (Figure 5).

Time is a key control in the preservation of bar packages in the model stratigraphy. The youngest bars are the most likely to be preserved (Figure 4D) because they have a smaller likelihood of experiencing a channel reconfiguration that leads to erosion and reworking. This can be observed in Figure 5 where even small bars (smaller, shorter runs of localized deposition) end up as preserved bar packages in both stratigraphic cross sections. In natural systems, the youngest bed configuration can be preserved through channel-belt avulsion. When a reach is abandoned, the last bars occupying the channel bed will be left intact, barring reworking and modification from intermittent flow reoccupations or other floodplain processes, and will eventually be buried by floodplain deposits from neighboring channel-belts. Stopping the model run at different timesteps yields a similar variability in preservation in one cross-section as we observe at the end of the model run among all cross-sections (Figure 3C, Figure 5). For example, preservation assessed with different stoppage (avulsion) times for the two mapped cross sections evaluated in Figure 5 shows the proportion of fully and partially preserved bars ranging from 0% to 60% with no systematic variation over time (Figure S6). This range is comparable to the range of fully and partially preserved bars among all cross-sections at the end of the model run (17% to 68%; Figure 3C), emphasizing that local preservation will be highly variable from place to place and time to time, but observing preservation over multiple cross-sections provides constraints on the background stochastic variability of deposition in the channel belt.

The variability in preservation across different stopping (avulsion) times in one location in space, and at the same stopping time across all cross-sections provides insight into the nuances between local sediment storage and bypass, and avulsion in braided rivers. In the model, bars on the bed turn over on daily to monthly timescales, (average ~25 days). At times in sections when the rate of bar turnover is high relative to the rate of channel morphodynamics (i.e. higher local sediment storage), bar preservation may increase. Alternatively, if the rate of bar turnover is slow relative to the rate of morphodynamics like widening and thread migration, we anticipate a decrease in bar preservation. These observed dynamics are comparable with those documented in meandering systems in which preservation is controlled by the timing of both meander bend kinematics and avulsion (Durkin et al., 2018). The interaction of bar, channel-thread and channel-belt kinematics in the model highlight how the interaction of multiple scales of processes interact to influence preservation in multi-threaded systems, consistent with the concept of morphodynamic hierarchy controlling preservation in fluvial landscapes (Ganti et al., 2020). This indicates that comparing bar preservation across different systems provides an avenue for comparing the relative rates of channel-thread dynamics and avulsion timescales on ancient landscapes (e.g., Bristow & Best, 1993; Chamberlin & Hajek, 2019).

Implications for reconstructing landscape conditions from braided river deposits

Bar and channel deposits are important sources of information about paleoflow conditions in ancient rivers. Previous depth-scaling relationships suggest that fully preserved clinoform heights act as a proxy for paleo-flow depth (e.g., Alexander et al., 2020; Hajek & Heller, 2012; Mohrig et al., 2000). Our results corroborate that clinoforms from fully preserved bar clinothems provide a minimum estimate of the local maximum flow depth (scaling with 75% of the for-

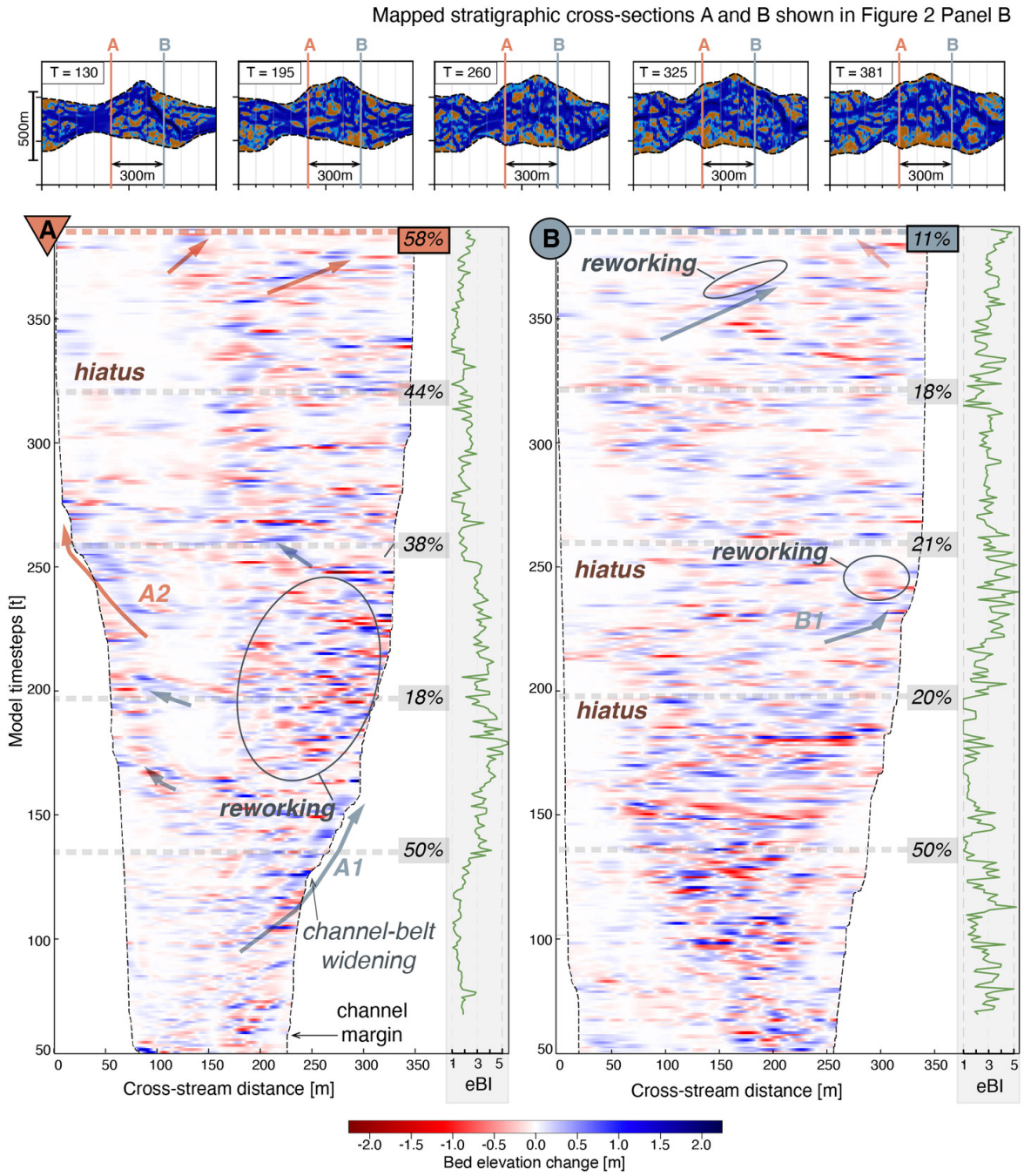

Figure 5. (Top) 1 km long reach of model domain showing bed evolution at 5 timesteps during the model run, and the locations of sections A (labelled with triangle) and B (labelled with circle). Stratigraphic cross-sections for sections A and B shown in Figure 2 Panel B. (Bottom) Chronostratigraphic bed event (erosion/deposition/hiatus) size and location diagram (Wheeler diagram) showing bed elevation change throughout the model run at for Section A (left) and Section B (right) with annotations describing the thread kinematics and formation of bars A1, A2 and B1 highlighted in Figure 2 Panel B. Arrows highlight example instances of sustained deposition. Grey numbered boxes in both diagrams indicate the percentage of preserved (fully and partially) bar packages in each cross-section if the model was stopped at the timesteps shown above (t = 130, 195, 260, 325, 381). Numbered boxes outlined in black indicate the percentage of preserved (fully and partially) packages in the final cross-sections (shown in Figure 2 Panel B) at the actual end of the model run, packages in Section A are mostly preserved while packages in Section B are primarily truncated. Green curves in the axes on the right of both bed event diagrams for section A and B show the trend in Entropic Braiding Index (eBI) at that section location throughout the model run (from the end of the model spin up period).

mative flow depth; Figure 4) and that on average the thickness of fully preserved bar packages reflects 90% the local maximum formative channel depth associated with bar deposition (Figure 4). Even partially preserved and truncated bar packages provide scale estimates of channel depth, albeit with more uncertainty. Fully preserved bar deposits can serve as important flow-depth constraints in ancient rivers, and depending on the precision required for paleohydraulic reconstructions (e.g., Hajek & Heller, 2012; Hartley & Owen, 2022; Lyster et al., 2021; Mahon & McElroy, 2018; Mohrig et al., 2000; Trampush et al., 2014), the scale of bar packages, regardless of preservation, can generally facilitate first-order comparisons of paleo-river size. This may be particularly useful in systems where outcrop extent and exposure limit our ability to collect these data in abundance (e.g., Ielpi et al., 2018) or in subsurface analyses in which seismic or well-log datasets limit spatial resolution (e.g., Bridge & Tye, 2000; Castelltort, 2018; Donselaar & Schmidt, 2005; Li et al., 2019; Yue et al., 2019).

In natural systems, channel flow conditions are reflected in the distribution of bed-material size and bedforms on the active riverbed (e.g., Ashworth et al., 1992; Southard & Boguchwal, 1990; Van Den Berg & Van Gelder, 1993). Although our pseudo-structures do not reflect specific bedform configurations, they serve as a proxy for how the spectrum of shear-stress conditions on the active bed are preserved stratigraphically, and are consistent with facies expectations of braided river deposits in ancient outcrops (e.g., Gibling, 2006; Lynds & Hajek, 2006; Miall, 1988). Deposits associated with low shear-stress conditions (regions of the channel with shallow flow depth and/or slow flow velocity) are commonly found within both preserved and truncated bars (Figure 2C) and can occupy up to 20% of some cross sections (Figure 3E). Intermediate flow conditions ("ripples" in our categorization) are present in stratigraphy in a similar proportion to the area they occupied on the bed during the model run (Figure 3D and E). High shear stress facies are overrepresented in stratigraphy relative to the area they occupy on the active channel bed (Figure 3D and 3E), likely because of greater sediment fluxes in zones of higher shear stress. The range of facies preservation in braided paleochannel deposits provides an opportunity to assess nuanced aspects of paleoflow conditions in ancient outcrops (e.g., Ashworth et al., 2011; Chamberlin & Hajek, 2022; Lynds & Hajek, 2006). Careful sampling across bar facies may provide important context for quantitative reconstructions of channel paleohydraulics (e.g., Hartley & Owen, 2022; Lyster et al., 2021, 2022, 2023; McLeod et al., 2023; Wood et al., 2023). More work is needed to fully elucidate how factors like flow variability and morphodynamic hierarchy control preservation of specific bed conditions in fluvial systems (e.g., Das et al., 2022; Ganti et al., 2020; Leary & Ganti, 2020; Lyster et al., 2022; Reesink et al., 2015), but the general consistency between mean, model bed, flow conditions and aggregate pseudo-structure abundance in stratigraphic cross-sections underscores the potential for robust comparisons of average or representative paleoflow conditions among ancient river systems.

Over the course of the model run, each segment of the river experienced the full suite of channel conditions (e.g., Entropic Braiding Index, shear stress distribution, and channel widening; Figure 3) observed in the model. Although each section has its own, independent history (Figure 5), with enough time, every location in the model domain exhibited the full range of flow configurations permissible given the model setup. It follows then that in field systems, provided that sufficient cross-sections and bar packages are sampled, aggregate data collected from braided river deposits can reflect estimates of the range of flow and preservation conditions present across the formative braid belt. As an example in our model, we can reproduce the average model preservation statistics, within one standard deviation of the mean, by averaging across a random sample of cross-sections (in this case, a minimum of 3, Figure S8). Furthermore, with a minimum random sample of 30 fully preserved bar packages, we can minimize the standard deviation in measurements of the proportion of flow depth recorded by preserved bar packages (Figure S9). These statistical observations suggest that these data can be used to robustly reconstruct minimum estimates of the range of flow conditions present in the formative river system. We note that this model provides one example braided river configuration. Future efforts should explore the degree to which internal stochasticity differs among rivers with different planforms (e.g., Galeazzi et al., 2021) and across different sediment supply, discharge variability, and bank stability conditions, and how these differences might manifest in ancient deposits.

Collectively, insights from this study can guide how we approach the stratigraphic record. Sampling multiple outcrops and averaging over multiple exposures and sand bodies from a paleochannel network can help provide accurate pictures of ancient landscapes. However, identifying subtle and precise differences between and among systems is likely challenging given differences in outcrop quality, exposure, and extent, and, as shown in this study, the inherently large degree of variability that should be expected within deposits of a single braided channel-belt. Comparing between localities and systems across clearly defined observation scales (e.g. channel-belt, bar package, bedform) and preservation trends can be useful. For example, insights from modeling in this study are consistent with preservation trends mapped in the Castlegate Formation where differences in preservation scale between localities were attributed to differences in avulsion-return time (where poorly preserved localities were associated with a relatively fast avulsion return time and well preserved localities were associated with a relatively long avulsion return time) (Chamberlin & Hajek, 2019). Field observations collected with the need for these statistical and geological consistencies in mind will help in comparing ancient systems at the bar and channel-belt scale. Furthermore, consistently mapped, and scaled field observations can contribute to broad community databases of ancient fluvial datasets that can improve analog selection for landscape reconstruction modeling, populating geologic models, and

predicting and assessing subsurface connectivity in braided river aquifers and reservoirs.

CONCLUSIONS

We used the model NAYS2DH (Jang & Shimizu, 2005; Nelson et al., 2016; Shimizu et al., 2011) to explore the relationship between channel kinematics and bar preservation in an unperturbed braided river system. Our data show that bar preservation in braided rivers is variable in both space and time and has no relationship to channel widening rate or braiding intensity as tested within the model. Ultimately, the rate of avulsion relative to the rate of bar turnover is the dominant control on bar preservation; this highlights the role of morphodynamic hierarchy in enhancing preservation of depositional elements in the stratigraphic record.

We find that the bar preservation and channel-belt stratigraphic architecture is the product of the unique history of channel-thread movements at each location on the bed, rather than being associated with specific types of channel movements or patterns. Our observations support two final takeaways: (1) bar clinoform and package geometries provide a reasonable estimate of the local maximum flow depth during bar formation; and (2) accurately categorizing and comparing the stratigraphic architecture and paleoflow conditions of ancient, braided river deposits will benefit from consistent mapping (i.e., across defined scales of observation) and extensive sampling. This insight will strengthen efforts to disentangle the impact of flow variability on fluvial deposits and predict facies variability and textural properties in buried braided river deposits.

ACKNOWLEDGEMENTS

This work was supported by funds from the National Science Foundation granted to Hajek (EAR-1935513). We thank Harrison Martin and two anonymous reviewers for their thoughtful comments and feedback that helped to improve our manuscript. Finally we would like to thank S. Lyster, R. DiBiase, D. Edmonds and R. Slingerland for insightful discussions.

Submitted: January 24, 2024 CDT, Accepted: April 26, 2024 CDT

References

Adams, M. M., & Bhattacharya, J. P. (2005). No Change in Fluvial Style Across a Sequence Boundary, Cretaceous Blackhawk and Castlegate Formations of Central Utah, U.S.A. *Journal of Sedimentary Research*, *75*, 1038–1051. https://doi.org/10.2110/jsr.2005.080

Alexander, J. S., McElroy, B. J., Huzurbazar, S., & Murr, M. L. (2020). Elevation gaps in fluvial sandbar deposition and their implications for paleodepth estimation. *Geology*, *48*, 718–722. https://doi.org/10.1130/G47521.1

Asahi, K., Shimizu, Y., Nelson, J., & Parker, G. (2013). Numerical simulation of river meandering with self-evolving banks. *Journal of Geophysical Research: Earth Surface*, *118*, 2208–2229. https://doi.org/10.1002/jgrf.20150

Ashworth, P. J., Ferguson, R. I., Ashmore, P. E., Paola, C., Powell, D. M., & Prestegaards, K. L. (1992). Measurements in a Braided River chute and lobe: 2. Sorting of bed load during entrainment, transport, and deposition. *Water Resources Research*, *28*, 1887–1896. https://doi.org/10.1029/92WR00702

Ashworth, P. J., Sambrook Smith, G. H., Best, J. L., Bridge, J. S., Lane, S. N., Lunt, Ian. A., Reesink, A. J. H., Simpson, C. J., & Thomas, R. E. (2011). Evolution and sedimentology of a channel fill in the sandy braided South Saskatchewan River and its comparison to the deposits of an adjacent compound bar: Evolution and sedimentology of a channel fill in a sandy braided river. *Sedimentology*, *58*, 1860–1883. https://doi.org/10.1111/j.1365-3091.2011.01242.x

Barefoot, E. A., Nittrouer, J. A., Foreman, B. Z., Hajek, E. A., Dickens, G. R., Baisden, T., & Toms, L. (2022). Evidence for enhanced fluvial channel mobility and fine sediment export due to precipitation seasonality during the Paleocene-Eocene thermal maximum. *Geology*, *50*, 116–120. https://doi.org/10.1130/G49149.1

Best, J. L., Ashworth, P. J., Bristow, C. S., & Roden, J. (2003). Three-Dimensional Sedimentary Architecture of a Large, Mid-Channel Sand Braid Bar, Jamuna River, Bangladesh. *Journal of Sedimentary Research*, *73*, 516–530. https://doi.org/10.1306/010603730516

Bradley, R. W., & Venditti, J. G. (2017). Reevaluating dune scaling relations. *Earth-Science Reviews*, *165*, 356–376. https://doi.org/10.1016/j.earscirev.2016.11.004

Bradley, R. W., & Venditti, J. G. (2021). Mechanisms of Dune Growth and Decay in Rivers. *Geophysical Research Letters*, *48*, e2021GL094572. https://doi.org/10.1029/2021GL094572

Bridge, J. S. (1993). Description and interpretation of fluvial deposits: a critical perspective. *Sedimentology*, *40*, 801–810. https://doi.org/10.1111/j.1365-3091.1993.tb01361.x

Bridge, J. S. (1997). Thickness of sets of cross strata and planar strata as a function of formative bed-wave geometry and migration, and aggradation rate. *Geology*, *25*, 971. https://doi.org/10.1130/0091-7613(1997)025

Bridge, J. S., & Lunt, I. A. (2006). Depositional Models of Braided Rivers. In *Braided Rivers* (pp. 11–50). John Wiley & Sons, Ltd. https://doi.org/10.1002/9781444304374.ch2

Bridge, J. S., & Tye, R. S. (2000). Interpreting the Dimensions of Ancient Fluvial Channel Bars, Channels, and Channel Belts from Wireline-Logs and Cores. *AAPG Bulletin*, *84*. https://doi.org/10.1306/A9673C84-1738-11D7-8645000102C1865D

Bristow, C. S., & Best, J. L. (1993). Braided rivers: perspectives and problems. *Geological Society, London, Special Publications*, *75*, 1–11. https://doi.org/10.1144/GSL.SP.1993.075.01.01

Cardenas, B. T., Lamb, M. P., Jobe, Z. R., Mohrig, D., & Swartz, J. M. (2023). Morphodynamic Preservation of Fluvial Channel Belts. *The Sedimentary Record*, *21*. https://doi.org/10.2110/001c.66285

Cardenas, B. T., Mohrig, D., Goudge, T. A., Hughes, C. M., Levy, J. S., Swanson, T., Mason, J., & Zhao, F. (2020). The anatomy of exhumed river-channel belts: Bedform to belt-scale river kinematics of the Ruby Ranch Member, Cretaceous Cedar Mountain Formation, Utah, USA. *Sedimentology*, *67*, 3655–3682. https://doi.org/10.1111/sed.12765

Castelltort, S. (2018). Empirical relationship between river slope and the elongation of bars in braided rivers: A potential tool for paleoslope analysis from subsurface data. *Marine and Petroleum Geology*, *96*, 544–550. https://doi.org/10.1016/j.marpetgeo.2018.05.008

Chadwick, A. J., Steele, S., Silvestre, J., & Lamb, M. P. (2022). Effect of Sea-Level Change on River Avulsions and Stratigraphy for an Experimental Lowland Delta. *Journal of Geophysical Research: Earth Surface*, *127*, e2021JF006422. https://doi.org/10.1029/2021JF006422

Chamberlin, E. P., & Hajek, E. A. (2015). Interpreting Paleo-Avulsion Dynamics from Multistory Sand Bodies. *Journal of Sedimentary Research*, *85*, 82–94. https://doi.org/10.2110/jsr.2015.09

Chamberlin, E. P., & Hajek, E. A. (2019). Using bar preservation to constrain reworking in channel-dominated fluvial stratigraphy. *Geology*, *47*, 531–534. https://doi.org/10.1130/G46046.1

Chamberlin, E. P., & Hajek, E. A. (2022). Fine-sediment Supply Can Control Fluvial Deposit Architecture: An Example From the Blackhawk Formation-Castlegate Sandstone Transition, Upper Cretaceous, Utah, USA. *The Sedimentary Record*, *20*. https://doi.org/10.2110/001c.36334

Colombera, L., Mountney, N. P., Russell, C. E., Shiers, M. N., & McCaffrey, W. D. (2017). Geometry and compartmentalization of fluvial meander-belt reservoirs at the bar-form scale: Quantitative insight from outcrop, modern and subsurface analogues. *Marine and Petroleum Geology*, *82*, 35–55. https://doi.org/10.1016/j.marpetgeo.2017.01.024

Das, D., Ganti, V., Bradley, R., Venditti, J., Reesink, A., & Parsons, D. R. (2022). The Influence of Transport Stage on Preserved Fluvial Cross Strata. *Geophysical Research Letters*, *49*, e2022GL099808. https://doi.org/10.1029/2022GL099808

Dixon, S. J., Sambrook Smith, G. H., Best, J. L., Nicholas, A. P., Bull, J. M., Vardy, M. E., Sarker, M. H., & Goodbred, S. (2018). The planform mobility of river channel confluences: Insights from analysis of remotely sensed imagery. *Earth-Science Reviews*, *176*, 1–18. https://doi.org/10.1016/j.earscirev.2017.09.009

Donselaar, M. E., & Schmidt, J. M. (2005). Integration of outcrop and borehole image logs for high-resolution facies interpretation: example from a fluvial fan in the Ebro Basin, Spain. *Sedimentology*, *52*, 1021–1042. https://doi.org/10.1111/j.1365-3091.2005.00737.x

Durkin, P. R., Boyd, R. L., Hubbard, S. M., Shultz, A. W., & Blum, M. D. (2017). Three-Dimensional Reconstruction of Meander-Belt Evolution, Cretaceous McMurray Formation, Alberta Foreland Basin, Canada. *Journal of Sedimentary Research*, *87*, 1075–1099. https://doi.org/10.2110/jsr.2017.59

Durkin, P. R., Hubbard, S. M., Holbrook, J., & Boyd, R. (2018). Evolution of fluvial meander-belt deposits and implications for the completeness of the stratigraphic record. *GSA Bulletin*, *130*, 721–739. https://doi.org/10.1130/B31699.1

Fielding, C. R. (2022). *Sedimentology and Stratigraphy of Large River Deposits: Recognition and Preservation Potential in the Rock Record, in Large Rivers*. John Wiley & Sons, Ltd. https://doi.org/10.1002/9781119412632.ch7

Fielding, C. R., Alexander, J., & Allen, J. P. (2018). The role of discharge variability in the formation and preservation of alluvial sediment bodies. *Sedimentary Geology*, *365*, 1–20. https://doi.org/10.1016/j.sedgeo.2017.12.022

Foreman, B. Z. (2014). Climate-driven generation of a fluvial sheet sand body at the Paleocene-Eocene boundary in north-west Wyoming (USA). *Basin Research*, *26*, 225–241. https://doi.org/10.1111/bre.12027

Foreman, B. Z., Heller, P. L., & Clementz, M. T. (2012). Fluvial response to abrupt global warming at the Palaeocene/Eocene boundary. *Nature*, *491*, 92–95. https://doi.org/10.1038/nature11513

Galeazzi, C. P., Almeida, R. P., & do Prado, A. H. (2021). Linking rivers to the rock record: Channel patterns and paleocurrent circular variance. *Geology*, *49*, 1402–1407. https://doi.org/10.1130/G49121.1

Ganti, V., Hajek, E. A., Leary, K., Straub, K. M., & Paola, C. (2020). Morphodynamic Hierarchy and the Fabric of the Sedimentary Record. *Geophysical Research Letters*, *47*. https://doi.org/10.1029/2020GL087921

Ganti, V., Paola, C., & Foufoula-Georgiou, E. (2013). Kinematic controls on the geometry of the preserved cross sets. *Journal of Geophysical Research: Earth Surface*, *118*, 1296–1307. https://doi.org/10.1002/jgrf.20094

Germanoski, D., & Schumm, S. A. (1993). Changes in Braided River Morphology Resulting from Aggradation and Degradation. *The Journal of Geology*, *101*, 451–466. https://doi.org/10.1086/648239

Ghosh, S., Mandal, P., & Bera, B. (2023). Dynamics of channel bar morphology on multi-decadal timescales in a braided river within Himalayan foreland basin, India. *Journal of Earth System Science*, *132*, 168. https://doi.org/10.1007/s12040-023-02187-x

Gibling, M. R. (2006). Width and Thickness of Fluvial Channel Bodies and Valley Fills in the Geological Record: A Literature Compilation and Classification. *Journal of Sedimentary Research*, *76*, 731–770. https://doi.org/10.2110/jsr.2006.060

Guo, W., Dong, C., Lin, C., Zhang, T., Zhao, Z., & Li, J. (2022). 3D Sedimentary Architecture of Sandy Braided River, Based on Outcrop, Unmanned Aerial Vehicle and Ground Penetrating Radar Data. *Minerals*, *12*, 739. https://doi.org/10.3390/min12060739

Hajek, E. A., & Heller, P. L. (2012). Flow-Depth Scaling In Alluvial Architecture and Nonmarine Sequence Stratigraphy: Example from the Castlegate Sandstone, Central Utah, U.S.A. *Journal of Sedimentary Research*, *82*, 121–130. https://doi.org/10.2110/jsr.2012.8

Hajek, E. A., Huzurbazar, S. V., Mohrig, D., Lynds, R. M., & Heller, P. L. (2010). Statistical Characterization of Grain-Size Distributions in Sandy Fluvial Systems. *Journal of Sedimentary Research*, *80*, 184–192. https://doi.org/10.2110/jsr.2010.020

Hartley, A. J., & Owen, A. (2022). Paleohydraulic analysis of an ancient distributive fluvial system. *Journal of Sedimentary Research*, *92*, 445–459. https://doi.org/10.2110/jsr.2021.062

Hartley, A. J., Owen, A., Swan, A., Weissmann, G. S., Holzweber, B. I., Howell, J., Nichols, G., & Scuderi, L. (2015). Recognition and importance of amalgamated sandy meander belts in the continental rock record. *Geology*, *43*, 679–682. https://doi.org/10.1130/G36743.1

Heller, P. L., & Paola, C. (1996). Downstream changes in alluvial architecture; an exploration of controls on channel-stacking patterns. *Journal of Sedimentary Research*, *66*, 297–306. https://doi.org/10.1306/D4268333-2B26-11D7-8648000102C1865D

Holbrook, J., & Wanas, H. (2014). A Fulcrum Approach To Assessing Source-To-Sink Mass Balance Using Channel Paleohydrologic Paramaters Derivable From Common Fluvial Data Sets With An Example From the Cretaceous of Egypt. *Journal of Sedimentary Research*, *84*, 349–372. https://doi.org/10.2110/jsr.2014.29

Ielpi, A., Ghinassi, M., Rainbird, R. H., & Ventra, D. (2018). Planform sinuosity of Proterozoic rivers. In *Fluvial Meanders and Their Sedimentary Products in the Rock Record* (pp. 81–118). John Wiley & Sons, Ltd. https://doi.org/10.1002/9781119424437.ch4

Ielpi, A., Lapôtre, M. G. A., Gibling, M. R., & Boyce, C. K. (2022). The impact of vegetation on meandering rivers. *Nature Reviews Earth & Environment*, *3*, 165–178. https://doi.org/10.1038/s43017-021-00249-6

Jang, C.-L., & Shimizu, Y. (2005). Numerical Simulation of Relatively Wide, Shallow Channels with Erodible Banks. *Journal of Hydraulic Engineering*, *131*, 565–575. https://doi.org/10.1061/(ASCE)0733-9429(2005)131:7(565)

Jarriel, T., Swartz, J., & Passalacqua, P. (2021). Global rates and patterns of channel migration in river deltas. *Proceedings of the National Academy of Sciences*, *118*, e2103178118. https://doi.org/10.1073/pnas.2103178118

Jerolmack, D. J., & Mohrig, D. (2005). A unified model for subaqueous bed form dynamics. *Water Resources Research*, *41*. https://doi.org/10.1029/2005WR004329

Kleinhans, M. G., & van den Berg, J. H. (2011). River channel and bar patterns explained and predicted by an empirical and a physics-based method. *Earth Surface Processes and Landforms*, *36*, 721–738. https://doi.org/10.1002/esp.2090

Le Guern, J., Rodrigues, S., Tassi, P., Cordier, F., Wintenberger, C. L., & Jugé, P. (2023). Migrating bars influence the formation and dynamics of their peers in large sandy-gravel bed rivers. *Earth Surface Processes and Landforms*, *1*, 1–14. https://doi.org/10.1002/esp.5563

Leary, K. C. P., & Ganti, V. (2020). Preserved Fluvial Cross Strata Record Bedform Disequilibrium Dynamics. *Geophysical Research Letters*, *47*. https://doi.org/10.1029/2019GL085910

Leclair, S. F., Bridge, J. S., & Wang, F. Q. (1997). Preservation of cross-strata due to migration of subaqueous dunes over aggrading and non-aggrading beds: Comparison of experimental data with theory. *Geoscience Canada*, *24*, 55–66.

Lewis, K. D., Pranter, M. J., Reza, Z. A., & Cole, R. D. (2018). Fluvial architecture of the Burro Canyon Formation using UAV-based photogrammetry and outcrop-based modeling: implications for reservoir performance, Rattlesnake Canyon, southwestern Piceance Basin, Colorado. *The Sedimentary Record*, *16*, 4–10. https://doi.org/10.2110/sedred.2018.3.4

Li, W., Colombera, L., Yue, D., & Mountney, N. P. (2023). Controls on the morphology of braided rivers and braid bars: An empirical characterization of numerical models. *Sedimentology*, *70*, 259–279. https://doi.org/10.1111/sed.13040

Li, W., Yue, D., Wang, W., Wang, W., Wu, S., Li, J., & Chen, D. (2019). Fusing multiple frequency-decomposed seismic attributes with machine learning for thickness prediction and sedimentary facies interpretation in fluvial reservoirs. *Journal of Petroleum Science and Engineering*, *177*, 1087–1102. https://doi.org/10.1016/j.petrol.2019.03.017

Lunt, I. A., Bridge, J. S., & Tye, R. S. (2004). A quantitative, three-dimensional depositional model of gravelly braided rivers. *Sedimentology*, *51*, 377–414. https://doi.org/10.1111/j.1365-3091.2004.00627.x

Lynds, R., & Hajek, E. (2006). Conceptual model for predicting mudstone dimensions in sandy braided-river reservoirs. *AAPG Bulletin*, *90*, 1273–1288. https://doi.org/10.1306/03080605051

Lyster, S. J., Whittaker, A. C., Farnsworth, A., & Hampson, G. J. (2023). Constraining flow and sediment transport intermittency in the geological past. *Geological Society of America Bulletin*, *130*. https://doi.org/10.1130/B36873.1

Lyster, S. J., Whittaker, A. C., Hajek, E. A., & Ganti, V. (2022). Field evidence for disequilibrium dynamics in preserved fluvial cross-strata: A record of discharge variability or morphodynamic hierarchy? *Earth and Planetary Science Letters*, *579*, 117355. https://doi.org/10.1016/j.epsl.2021.117355

Lyster, S. J., Whittaker, A. C., Hampson, G. J., Hajek, E. A., Allison, P. A., & Lathrop, B. A. (2021). Reconstructing the morphologies and hydrodynamics of ancient rivers from source to sink: Cretaceous Western Interior Basin, Utah, USA. *Sedimentology*, *68*, 2854–2886. https://doi.org/10.1111/sed.12877

Mahon, R. C., & McElroy, B. (2018). Indirect estimation of bedload flux from modern sand-bed rivers and ancient fluvial strata. *Geology*, *46*, 579–582. https://doi.org/10.1130/G40161.1

Martin, B., Owen, A., Nichols, G. J., Hartley, A. J., & Williams, R. D. (2021). Quantifying Downstream, Vertical and Lateral Variation in Fluvial Deposits: Implications From the Huesca Distributive Fluvial System. *Frontiers in Earth Science*, *8*, 564017. https://doi.org/10.3389/feart.2020.564017

Martin, J., Paola, C., Abreu, V., Neal, J., & Sheets, B. (2009). Sequence stratigraphy of experimental strata under known conditions of differential subsidence and variable base level. *AAPG BULLETIN*, *93*, 503–533. https://doi.org/10.1306/12110808057

McLaurin, B. T., & Steel, R. J. (2007). Architecture and origin of an amalgamated fluvial sheet sand, lower Castlegate Formation, Book Cliffs, Utah. *Sedimentary Geology*, *197*, 291–311. https://doi.org/10.1016/j.sedgeo.2006.10.005

McLeod, J. S., Wood, J., Lyster, S. J., Valenza, J. M., Spencer, A. R. T., & Whittaker, A. C. (2023). Quantitative constraints on flood variability in the rock record. *Nature Communications*, *14*, 3362. https://doi.org/10.1038/s41467-023-38967-8

McMahon, W. J., & Davies, N. S. (2018). Evolution of alluvial mudrock forced by early land plants. *Science*, *359*, 1022–1024. https://doi.org/10.1126/science.aan4660

Miall, A. D. (1985). Architectural-Element Analysis: A New Method of Facies Analysis Applied to Fluvial Deposits. *Earth-Science Reviews*, *22*, 261–308. https://doi.org/10.1016/0012-8252(85)90001-7

Miall, A. D. (1988). Architectural elements and bounding surfaces in fluvial deposits: anatomy of the Kayenta formation (lower jurassic), Southwest Colorado. *Sedimentary Geology*, *55*, 233–262. https://doi.org/10.1016/0037-0738(88)90133-9

Miall, A. D. (1994). Reconstructing Fluvial Macroform Architecture from Two-Dimensional Outcrops: Examples from the Castlegate Sandstone, Book Cliffs, Utah. *SEPM Journal of Sedimentary Research*, *64B*. https://doi.org/10.1306/D4267F78-2B26-11D7-8648000102C1865D

Mohrig, D., Heller, P. L., Paola, C., & Lyons, W. J. (2000). Interpreting avulsion process from ancient alluvial sequences: Guadalope-Matarranya system (northern Spain) and Wasatch Formation (western Colorado). *Geological Society of America Bulletin*.

Myrow, P. M., Jerolmack, D. J., & Perron, J. T. (2018). Bedform Disequilibrium. *Journal of Sedimentary Research*, *88*, 1096–1113. https://doi.org/10.2110/jsr.2018.55

Nelson, J. M. (2016). The international river interface cooperative: Public domain flow and morphodynamics software for education and applications. *Advances in Water Resources*, *93*, 62–74. https://doi.org/10.1016/j.advwatres.2015.09.017

Owen, A., Nichols, G. J., Hartley, A. J., Weissmann, G. S., & Scuderi, L. A. (2015). Quantification of a Distributive Fluvial System: The Salt Wash DFS of the Morrison Formation, SW U.S.A. *Journal of Sedimentary Research*, *85*, 544–561. https://doi.org/10.2110/jsr.2015.35

Paola, C., & Borgman, L. (1991). Reconstructing random topography from preserved stratification. *Sedimentology*, *38*, 553–565. https://doi.org/10.1111/j.1365-3091.1991.tb01008.x

Paola, C., Straub, K., Mohrig, D., & Reinhardt, L. (2009). The "unreasonable effectiveness" of stratigraphic and geomorphic experiments. *Earth-Science Reviews*, *97*, 1–43. https://doi.org/10.1016/j.earscirev.2009.05.003

Rahman, M. R. (2023). River dynamics – a geospatial analysis of Jamuna (Brahmaputra) River in Bangladesh during 1973–2019 using Landsat satellite remote sensing data and GIS. *Environmental Monitoring and Assessment*, *195*, 96. https://doi.org/10.1007/s10661-022-10638-z

Reesink, A. J. H., Van den Berg, J. H., Parsons, D. R., Amsler, M. L., Best, J. L., Hardy, R. J., Orfeo, O., & Szupiany, R. N. (2015). Extremes in dune preservation: Controls on the completeness of fluvial deposits. *Earth-Science Reviews*, *150*, 652–665. https://doi.org/10.1016/j.earscirev.2015.09.008

Rice, S. P., Church, M., Wooldridge, C. L., & Hickin, E. J. (2009). Morphology and evolution of bars in a wandering gravel-bed river; lower Fraser river, British Columbia, Canada. *Sedimentology*, *56*, 709–736. https://doi.org/10.1111/j.1365-3091.2008.00994.x

Sahoo, H., Gani, M. R., Gani, N. D., Hampson, G. J., Howell, J. A., Storms, J. E. A., Martinius, A. W., & Buckley, S. J. (2020). Predictable patterns in stacking and distribution of channelized fluvial sand bodies linked to channel mobility and avulsion processes. *Geology*, *48*, 903–907. https://doi.org/10.1130/G47236.1

Sambrook Smith, G. H., Best, J. L., Ashworth, P. J., Lane, S. N., Parker, N. O., Lunt, I. A., Thomas, R. E., & Simpson, C. J. (2010). Can we distinguish flood frequency and magnitude in the sedimentological record of rivers? *Geology*, *38*, 579–582. https://doi.org/10.1130/G30861.1

Sambrook Smith, G. H., Nicholas, A. P., Best, J. L., Bull, J. M., Dixon, S. J., Goodbred, S., Sarker, M. H., & Vardy, M. E. (2019). The sedimentology of river confluences. *Sedimentology*, *66*, 391–407. https://doi.org/10.1111/sed.12504

Schuurman, F., & Kleinhans, M. G. (2015). Bar dynamics and bifurcation evolution in a modelled braided sand-bed river: Bar dynamics and bifurcation evolution in a modelled braided sand-bed river. *Earth Surface Processes and Landforms*, *40*, 1318–1333. https://doi.org/10.1002/esp.3722

Schuurman, F., Kleinhans, M. G., & Middelkoop, H. (2016). Network response to disturbances in large sand-bed braided rivers. *Earth Surface Dynamics*, *4*, 25–45. https://doi.org/10.5194/esurf-4-25-2016

Sharma, N., Whittaker, A. C., Watkins, S. E., Valero, L., Vérité, J., Puigdefabregas, C., Adatte, T., Garcés, M., Guillocheau, F., & Castelltort, S. (2023). Water discharge variations control fluvial stratigraphic architecture in the Middle Eocene Escanilla formation, Spain. *Scientific Reports*, *13*, 6834. https://doi.org/10.1038/s41598-023-33600-6

Shimizu, Y., Takebayashi, H., Inoue, T., Hamaki, M., Iwasaki, T., & Nabi, M. (2011). *NAYS2DH Solver Manual*. https://i-ric.org/en/download/nays2dh-menual-v3/

Smith, D. G., Hubbard, S. M., Lavigne, J. R., Leckie, D. A., & Fustic, M. (2011). Stratigraphy of Counter-Point-Bar and Eddy-Accretion Deposits in Low-Energy Meander Belts of the Peace-Athabasca Delta, Northeast Alberta, Canada. In S. K. Davidson, S. Leleu, & C. P. North (Eds.), *From River to Rock Record: The preservation of fluvial sediments and their subsequent interpretation* (Vol. 97, p. 0). SEPM Society for Sedimentary Geology. https://doi.org/10.2110/sepmsp.097.143

Southard, J. B., & Boguchwal, L. A. (1990). *Bed Configurations in Steady Unidirectional Water Flows. Part 2. Synthesis of Flume Data*. https://doi.org/10.1306/212F9241-2B24-11D7-8648000102C1865D

Straub, K. M., & Wang, Y. (2013). Influence of water and sediment supply on the long-term evolution of alluvial fans and deltas: Statistical characterization of basin-filling sedimentation patterns: Basin Filling Sedimentation Patterns. *Journal of Geophysical Research: Earth Surface*, *118*, 1602–1616. https://doi.org/10.1002/jgrf.20095

Strong, N., Sheets, B., Hickson, T., & Paola, C. (2005). A mass-balance framework for quantifying downstream changes in fluvial architecture. In M. D. Blum, S. B. Marriott, & S. F. Leclair (Eds.), *Fluvial Sedimentology VII* (pp. 243–253). Blackwell Publishing Ltd. https://doi.org/10.1002/9781444304350.ch14

Sylvester, Z., Durkin, P. R., Hubbard, S. M., & Mohrig, D. (2021). Autogenic translation and counter point bar deposition in meandering rivers. *GSA Bulletin*, *133*, 2439–2456. https://doi.org/10.1130/B35829.1

Tejedor, A., Schwenk, J., Kleinhans, M., Limaye, A. B., Vulis, L., Carling, P., Kantz, H., & Foufoula-Georgiou, E. (2022). The Entropic Braiding Index (eBI): A Robust Metric to Account for the Diversity of Channel Scales in Multi-Thread Rivers. *Geophysical Research Letters*, *49*, e2022GL099681. https://doi.org/10.1029/2022GL099681

Trampush, S. M., Huzurbazar, S., & McElroy, B. (2014). Empirical assessment of theory for bankfull characteristics of alluvial channels. *Water Resources Research*, *50*, 9211–9220. https://doi.org/10.1002/2014WR015597

van de Lageweg, W. I., Schuurman, F., Cohen, K. M., van Dijk, W. M., Shimizu, Y., & Kleinhans, M. G. (2016). Preservation of meandering river channels in uniformly aggrading channel belts. *Sedimentology*, *63*, 586–608. https://doi.org/10.1111/sed.12229

van de Lageweg, W. I., van Dijk, W. M., Box, D., & Kleinhans, M. G. (2016). Archimetrics: a quantitative tool to predict three-dimensional meander belt sandbody heterogeneity. *The Depositional Record*, *2*, 22–46. https://doi.org/10.1002/dep2.12

Van Den Berg, J. H., & Van Gelder, A. (1993). A New Bedform Stability Diagram, with Emphasis on the Transition of Ripples to Plane Bed in Flows over Fine Sand and Silt. In M. Marzo & C. Puigdefbregas (Eds.), *Alluvial Sedimentation* (pp. 11–21). Blackwell Publishing Ltd. https://doi.org/10.1002/9781444303995.ch2

Wickert, A. D., Martin, J. M., Tal, M., Kim, W., Sheets, B., & Paola, C. (2013). River channel lateral mobility: metrics, time scales, and controls. *Journal of Geophysical Research: Earth Surface*, *118*, 396–412. https://doi.org/10.1029/2012JF002386

Wintenberger, C. L., Rodrigues, S., Claude, N., Jugé, P., Bréhéret, J.-G., & Villar, M. (2015). Dynamics of nonmigrating mid-channel bar and superimposed dunes in a sandy-gravelly river (Loire River, France). *Geomorphology*, *248*, 185–204. https://doi.org/10.1016/j.geomorph.2015.07.032

Wood, J., McLeod, J. S., Lyster, S. J., & Whittaker, A. C. (2023). Rivers of the Variscan Foreland: fluvial morphodynamics in the Pennant Formation of South Wales, UK. *Journal of the Geological Society*, *180*, jgs2022-048. https://doi.org/10.1144/jgs2022-048

Yue, D., Li, W., Wang, W., Hu, G., Qiao, H., Hu, J., Zhang, M., & Wang, W. (2019). Fused spectral-decomposition seismic attributes and forward seismic modelling to predict sand bodies in meandering fluvial reservoirs. *Marine and Petroleum Geology*, *99*, 27–44. https://doi.org/10.1016/j.marpetgeo.2018.09.031

Supplementary Materials

Supplementary Material

Download: https://thesedimentaryrecord.scholasticahq.com/article/117787-the-fate-of-bars-in-braided-rivers/attachment/228034.pdf